Elastic strains and enhanced stress relaxation effects induced by ion irradiation in W(110)/Cu(111) multilayers: Comparative EXAFS and x-ray diffraction studies

M. Jaouen,* J. Pacaud, and C. Jaouen

Laboratoire de Métallurgie Physique, UMR 6630 du CNRS, Université de Poitiers SP2MI, Téléport 2, Bd Pierre et Marie Curie, Boite Postale 30179, 86962 Futuroscope Chasseneuil Cedex, France

(Received 26 February 2001; published 21 September 2001)

A characterization of the local structure in Cu/W superlattices (period $\Lambda = 20$ nm) prepared by ion beam sputtering with average composition $Cu_{50}W_{50}$ has been performed by x-ray absorption spectroscopy (EXAFS) and x-ray diffraction (XRD). Copper and tungsten are immiscible and so, sharp concentration modulation is obtained. The elasticity analysis of the EXAFS data evidences the existence of large strains due to compressive stress in the growth planes of W sublayers. The stress level determinated from EXAFS agrees fairly well with the one deduced from XRD while lattice parameters obtained from EXAFS are smaller than those measured with XRD. This discrepancy can be attributed to the inherent differences between short-range and long-range order methods for probing the material, but also to the limited accuracy of the EXAFS method for determining lattice parameters. However, EXAFS is well suited to the study of the disorder inside each elemental components of these superlattices. After an irradiation with a low Kr ions dose (10^{13} ions/cm^2), the W sublayers are partially relaxed to a stress level equal to one half of its original value while the structure of the Cu remains unchanged. The combination of the EXAFS and XRD techniques is a unique approach to achieve a complete characterization of the structural properties of strained nanometric layers as those considered in the present paper.

DOI: 10.1103/PhysRevB.64.144106 PACS number(s): 68.65.−k, 61.10.Ht, 61.82.Bg, 62.40.+i

I. INTRODUCTION

Recently, much interest has been devoted to the study of metallic multilayers due to their unusual physical and mechanical properties. Thus, drastically reduced shear modulus and significantly enhanced biaxial and Young moduli have been observed in some metallic systems when the periodicity length of the compositional modulation is decreasing.[1] It is generally accepted[2] that these elastic anomalies are correlated with the extreme strain states of the constituents resulting from bulk or interfacial effects. Several explanations based on electronic[3,4] or structural arguments[5–7] have been proposed in the last few years to explain the elastic anomalies of superlattices. To obtain a better understanding of such anomalous physical properties, the issue of the stress-strain relation in multilayered systems is essential. In this respect, x-ray scattering method has been demonstrated to be an efficient technique for determining strain and stress, e.g., the elastic response of the constituents.[8,9] Moreover, by measuring independently the stress in the different layers by x-ray diffraction (XRD) and the force applied by the modulated structure on the substrate via the measurement of its curvature, the interfacial contribution stress[10–12] can also be estimated. For nonepitaxial thin films with nanometric thicknesses, such as those often obtained by the sputtering technique, strain measurements often raise some experimental difficulties. Indeed, due to texture and mosaicity effects, a large spreading of the intensity of the asymmetric diffraction lines makes their apparition rather difficult and consequently a detailed strain-stress analysis turns out to be rather delicate and inaccurate. A second difficulty is related to the scattering method that probes ordered regions within the coherence length of the beam and that consequently does not account for stresses present in disordered areas.

In a previous paper,[13] a determination of the strain state of W layers in textured Cu/W multilayers elaborated by the sputtering method with a modulation wavelength of 7.5 nm was performed by XRD. It was more particularly shown that the individual tungsten layers sustain considerable elastic strains, far above the yield strain reported for bulk metal, due to the presence of residual compressive stresses (≈ -6 GPa). Such large strains developed in tungsten seem to account for the total out-of-plane expansion ($\approx +0.9\%$) of the average lattice spacing of the superlattice. A whole understanding of the complete strain-stress state of these multilayers to get some insight into the possible relation with the elastic softening observed in this system[14] also requires that we obtain structural information about copper layers.

Extended x-ray absorption fine structure (EXAFS) spectroscopy is a well-suited technique for structural characterization of solids. It can also be, in proper cases, a versatile method for determining strain and stress, e.g., the elastic response of materials and more especially that of multilayers. Indeed, EXAFS is element selective: by recording a spectrum at the edge of a given element, one can get accurate information on its specific local crystallographic environment including the average coordination number N of the different surrounding atoms, their distances R to the absorber, as well as the spatial fluctuation of distances σ (Debye-Waller factors). Furthermore, using the linear polarization of the x-ray synchrotron radiation (SR), structural information both in-plane and out-of-plane with respect to the sample's surface can also be extracted through independent measurements. Up to now, this technique has been mainly used to determine the anisotropic structure of thin metastable epitaxial films.[15–20] However, each set of atomic distances deduced from an EXAFS analysis for each different first near neighboring shells can be viewed as an *in situ* local strain gauge and thus EXAFS potentially allows one to determine the stress state of the constituents of the probed

 ©2001 The American Physical Society

sample. The present work intends to obtain complementary information about local atomic order, e.g., on the short range structure, of the two elements constituting the Cu/W multilayers by performing EXAFS experiments. To check the sensitivity of this approach, a (111)Cu/(110)W multilayer which composition wavelength is large ($\Lambda = 20$ nm) has been selected to minimize at maximum the specific contribution of the interfacial environments to the EXAFS signals. Taking full advantage of the polarization properties of the SR, our purpose is to resolve the anisotropic strains both in the out-of-plane direction and in the plane of growth. An attempt to determine the residual stress state of the two sublayers will be presented for an as-deposited multilayer and after an ion induced stress relaxation has been performed. In the case of the W sublayers, the results will be compared to those deduced from a strain-stress analysis using XRD measurements. Therefore, the question which is mainly addressed in this paper is that of the origin for the strains observed in Cu/W multilayers deposited using an ion beam sputtering technique at the microscopic scale.

II. EXPERIMENTAL METHODS

A. Sample preparation

Cu/W multilayers were prepared in a sputtering deposition system equipped with a broad Kauffman ion source using an argon ion beam extracted under an acceleration voltage of 1.2 kV. The base pressure was about 10^{-4} Pa before initiating the growth and about 10^{-2} Pa ($\approx 8 \times 10^{-5}$ Torr) during deposition. The tungsten and copper layers are sputtered from pure metal targets (grade : 99.995%). Single-crystalline silicon wafers with the (100) orientation and fused quartz substrates, used for XRD and EXAFS measurements, respectively, were fixed on a rotating substrate holder. The deposition was carried out at room temperature. The deposition rates were controlled with a quartz oscillator. Their values, calibrated by preliminary thickness measurements using an x-ray reflectometry setup, were 3.6 nm/min for Cu and 1.2 nm/min for W. The multilayer consists of 5 periods of alternate W and Cu layers which thickness' ratio is adjusted to get a nominal 1:1 composition. The modulation wavelength $\Lambda = t_W + t_{Cu}$ as determined by small-angle XRD was 20.07 nm, t_W and t_{Cu} being the thickness of the W and Cu layers, respectively. Thus, the total thickness of the multilayer is ≈ 100.4 nm. Energy dispersive x-ray spectroscopy (EDX) measurement gives as overall composition $Cu_{55}W_{45}$ (within an uncertainty of $\pm 1\%$). Therefore, the layering pattern $[W_m/Cu_n]_N$, where m and n are the numbers of atomic stacking planes in the direction of growth for W and Cu sublayers and N the number of bilayers, can be noted $[W_{47}/Cu_{46}]_5$. Excepted for trapped Ar atoms coming from the sputtering beam ($\approx 0.7\%$), no impurities were detected from the EDX analysis.

B. Ion irradiation experiments

The samples were irradiated at liquid nitrogen temperature with 340 keV Kr^{2+} ions under a vacuum of about 2×10^{-5} Pa. The energy was selected so that the ions projected range slightly exceeds the total film thickness. In that case, the energy deposition is, within $\approx \pm 20\%$, nearly uniform throughout the whole film thickness. The ion current density was kept below 0.3 μA/cm^2 to avoid heating effects. The TRIM code[21] was used to calculate the dose, expressed in displacements per atom (dpa), assuming an average threshold energy of 50 eV. The value so obtained was 0.386 10^{-14} dpa/ion. The nuclear energy deposited per depth length unit was approximately equal to 5 keV/nm.

C. X-ray diffraction measurements

1. Strain measurements

The structure of the multilayer and strain measurements were carried out using two diffractometers. Symmetric reflection x-ray measurements were performed on a Siemens D501 powder diffractometer equipped with a backside monochromator and a proportional detector using Cu $K\alpha$ radiation. The XRD measurements were carried out in a high-angle 2θ region (37°–47°) around the (110) and (111) Bragg's peaks of the tungsten and copper layers, respectively. By tilting around the θ-2θ direction (ω scans) for the (110) W and (111) Cu reflections, a relatively good stacking of the dense packed planes was evidenced since the full width at half maximum (FWHM) of the rocking curves deduced from the ω scans is equal to 9° for both bcc and fcc structures, a result in good agreement with high resolution transmission electron microscopy (HRTEM) observations.[22] Asymmetric plane spacings were measured using a four circles diffractometer (Seifert XRD 3000) equipped with a Cu x-ray source, a fiber optics and an Eulerian cradle for ψ tilting, e.g., tilting of the sample around the axis defined by the intersection between the scattering plane and the sample surface. The focused incident beam size was 1×1 mm^2. The detector setup was defined by two slits (0.28° divergence), a flat graphite analyzer, and a proportional detector. The same diffractometer was also used, without the graphite analyzer, for grazing-incidence x-ray scattering (GIXS) measurements with a grazing angle of 2°. The peak positions were obtained from the scattering profiles by fitting a linear background and each peak to identical shaped $K\alpha_1$ and $K\alpha_2$ pseudo-Voigt profiles with a fixed intensity ratio. For each measured reflexion $\{hkl\}$, specimen tilt and rotation angles (ψ,ϕ), the lattice parameter was deduced from the average lattice spacing $d_{\psi,\phi}$ according to the Bragg law.

2. Strain determination

The XRD method for strain measurement is based on the determination of the average lattice plane spacing d_{hkl} of the stressed layer via the measurement of a specific $\{hkl\}$ reflexion recorded along a direction which is defined with respect to the specimen geometry by the Eulerian angles ψ and ϕ, where ψ denotes the tilt angle between the normals to the surface and to the diffracting planes while ϕ is the rotation angle between the projected lattice plane normal and a reference axis in the plane of the sample. For each measured reflexion $\{hkl\}$, the lattice strain in the direction described by the angles ψ and ϕ can be expressed according to

$$\epsilon_{\psi,\phi}=\frac{d_{\psi,\phi}-d_0}{d_0}, \quad (1)$$

where d_0 is the lattice spacing corresponding to a stress-free specimen. In multilayers or thin films, due to alloying or relaxation effects, the unstrained lattice parameter is not known accurately. Therefore, the strain cannot be obtained directly.

Strains and stresses in thin films are usually referenced to the sample reference frame defined by the vectors $(\vec{S}_1,\vec{S}_2,\vec{S}_3)$ where $\vec{S}_3$ denotes the direction of the thin film normal (e.g., the crystallographic growth texture axis), the two others being referenced in the plane with respect to the orientation of the crystallites axis. So the strain $\epsilon_{\psi,\phi}$ can be expressed as

$$\epsilon_{\psi,\phi}=\epsilon_{11}\cos^2\phi\sin^2\psi+\epsilon_{12}\sin 2\phi\sin^2\psi+\epsilon_{22}\sin^2\phi\sin^2\psi+\epsilon_{33}\cos^2\psi+\epsilon_{13}\cos\phi\sin 2\psi+\epsilon_{23}\sin\phi\sin 2\psi, \quad (2)$$

where $\epsilon_{\psi,\phi}$ refers to the sample reference frame. An elasticity analysis via the Hooke law allows to relate the strain tensor to the stress one (or vice versa) by the introduction of the stiffness or compliance tensors[23] through the well known relations $\sigma_i=c_{ij}\epsilon_j$; $\epsilon_j=s_{ij}\sigma_i$ where c_{ij} and s_{ij}, using Voigt's notations, are the elements of the stiffness and compliance tensors, respectively.

A detailed and useful presentation of the stress analysis for extracting the stress and unstrained lattice parameter from both uniformly oriented and cubic fiber-textured thin films has been given by Clemens and Bain.[9] In the case of textured films, it is assumed that all crystallites having the same orientation are considered as forming a unique crystal. This means that every crystallite is submitted to the same stress state which is the Reuss averaging scheme. Due to the specific geometry, a thin film deposited onto a substrate is free to expand or contract along the film normal direction. It results that the stress in this direction and shear components that involve the normal direction are equal to zero so that $\sigma_{33}=\sigma_{13}=\sigma_{23}=0$. In many cases, an equal-biaxial stress state is moreover observed $(\sigma=\sigma_{11}=\sigma_{22})$, consequently all shear components are also zero. Nevertheless, when an epitaxial relationship between crystalline lattices of different symmetry takes place, it appears a nonequal biaxial stress state. Such a situation is quite conceivable in the case of Cu(111)/W(110) multilayers.

For a layer which growth texture is (111) as it will be the case here for Cu layers, assuming the principal stress directions σ_{11} and σ_{22} to be along the directions $[\bar{1}10]$ and $[\bar{1}\bar{1}2]$ of the sample reference frame, the strain $\epsilon_{\psi,\phi}$ in an arbitrary direction defined by the angles ψ and ϕ is given by

$$\epsilon_{\psi,\phi}^{[111]}=(\sigma_{22}-\sigma_{11})\left[\frac{2s_{11}-2s_{12}-s_{44}}{6\sqrt{2}}\sin\phi\sin 2\psi+\frac{-s_{11}+s_{12}-s_{44}}{6}\cos 2\phi\sin^2\psi\right]+(\sigma_{22}+\sigma_{11})\times\left[\frac{2s_{11}+4s_{12}-s_{44}}{6}+\frac{s_{44}}{4}\sin^2\psi\right], \quad (3)$$

where the elastic compliance constants s_{ij} are expressed in the crystallographic reference frame defined from the basis vectors of the unit cell.

For a bcc material with a (110) texture as it will occur in W sublayers, a similar expression can be derived under the assumption that the principal stress directions σ_{11} and σ_{22} coincide with the main in-plane axis of the sample reference frame that are $[\bar{1}10]$ and $[001]$, respectively,

$$\epsilon_{\psi,\phi}^{[110]}=(\sigma_{22}-\sigma_{11})\left[\frac{-2s_{11}+2s_{12}-s_{44}}{8}+\left\{\frac{6s_{11}-6s_{12}-3s_{44}}{16}+\frac{-6s_{11}+6s_{12}-s_{44}}{16}\cos 2\phi\right\}\sin^2\psi\right]+(\sigma_{22}+\sigma_{11})\left[\frac{2s_{11}+6s_{12}-s_{44}}{8}+\left\{\frac{s_{44}}{4}+\frac{2s_{11}-2s_{12}-s_{44}}{8}\sin^2\phi\right\}\sin^2\psi\right]. \quad (4)$$

Thus, it appears that measurements at different distinct poles with the same azimuth ϕ result in a linear d versus $\sin^2\psi$ distribution. The above analysis refers to single crystalline grains; it implicitly assumes a known value of ϕ for each measured (hkl) reflexion. The mismatch between the twofold symmetry of the stress state and the threefold symmetry of the (111) fcc layers therefore implies that equivalent crystallographic directions in the same set $\{hkl\}$ can experiment different strains. In fiber textured (111) thin films, such reflexions are nevertheless undistinguishable. Indeed, for a given diffraction geometry, distinct $\{hkl\}$ reflexions belonging to different sets of crystallites contribute to the observed interference line and the d spacing will be averaged over all equivalent directions which otherwise cancel the term depending on $\sigma_{22}-\sigma_{11}$ in Eq. (3). For (110) textured bcc films, similar strains are obtained for equivalent crystallographic directions and consequently the x-ray measurement of the lattice spacing allows one to determine the stress components.

For the special case of tungsten layers, due to its mechanical isotropy $[s_{44}=2(s_{11}-s_{12})]$, some simplification of Eq. (4) occurs and it can be accordingly rewritten as

$$\epsilon_{\psi,\phi}^{\mathrm{W}[110]}=(\sigma_{22}-\sigma_{11})\left[\frac{-6s_{11}+6s_{12}-5s_{44}}{32}\cos 2\phi\sin^2\psi\right]+(\sigma_{22}+\sigma_{11})\left[\frac{2s_{11}+6s_{12}-s_{44}}{8}+\frac{s_{44}}{4}\sin^2\psi\right]. \quad (5)$$

From this, one can get[24] the ϕ-dependent "strain-free direction" ψ^*:

$$\sin^2\psi^*)_{\phi=0}=\frac{-s_{12}}{s_{11}-s_{12}}\left(1+\frac{\sigma_{22}}{\sigma_{11}}\right); \quad \sin^2\psi^*)_{\phi=\frac{\pi}{2}}=\frac{-s_{12}}{s_{11}-s_{12}}\left(1+\frac{\sigma_{11}}{\sigma_{22}}\right). \quad (6)$$

So the three unknowns σ_{11}, σ_{22} and the stress-free lattice

parameter a_0 can be deduced assuming that lattice spacings could be measured for a set of reflexions obtained for distinct ϕ directions belonging to the same crystallite-group.

D. EXAFS measurements and data analysis

The EXAFS experiments were performed at the Laboratoire pour l'Utilisation du Rayonnement Electromagnétique (LURE) at Orsay on the DCI storage ring operating at 1.85 GeV with a typical current of 250 mA. As the total thickness of our samples is limited to 100 nm, we use the conversion yield EXAFS (CEEXAFS) technique[25] that is well suited to the local analysis of thin samples. The Cu K (8879 eV) and W L_3 (10207 eV) edges data were stored on beam line D42 that is equipped with a Si (331) channel-cut single-crystal monochromator for energy tuning. The x-ray absorption spectra were recorded over about 1000 eV above the edges at liquid nitrogen temperature to reduce thermal disorder using a total electron yield device working in He gas at atmospheric pressure.[26] To assure a good signal-to-noise ratio, the electrons were collected over 2 s per data point, the energy step being 2 eV. The linear polarization of the SR gives access to anisotropic structural information since the local structure can be probed both in-plane and out-of-plane with respect to the sample surface. Thus, the EXAFS spectra of the multilayers were recorded in two geometries with respect to the sample surface that is, respectively, parallel and nearly perpendicular (77°) to the polarization direction of the x-ray beam. In that way, differences between the crystal structure in the plane of growth and in the growth direction can be revealed by recording the EXAFS spectra with the sample surface parallel and perpendicular to the polarization direction, respectively.[15–20]

All x-ray absorption spectra were analyzed in the same way following a now well-established procedure[27] to extract the EXAFS function from the data using the software developed by Michalowicz.[28] All spectra were at first background subtracted by extrapolating the pre-edge region with a linear function. They were then normalized in the same way using the Lengeler-Eisenberger method.[29] The EXAFS function $\chi(E)$ is defined as

$$\chi(E)=\frac{\mu(E)-\mu_0(E)}{\mu_0(E)}, \tag{7}$$

where $\mu(E)$ is the observed absorption coefficient of the probed element, and $\mu_0(E)$ is the atomic absorption coefficient. Since μ_0 cannot be observed experimentally, it was approximated by a fifth order polynomial passing through the data beyond the absorption edge. Once extracted from the data according to Eq. (7), $\chi(E)$ is converted in k space through the relation $k=\sqrt{2m(E-E_0)}/\hbar$ where the threshold energy E_0 is related to the Fermi energy which is considered in EXAFS as an adjustable parameter. After weighting in k^2, we take the Fourier transform (FT) of $k^2\chi(k)$ using a Kaiser apodisation window ($\tau=2.5$) which ends at two nodes of $\chi(k)$ chosen so that the δk range is as large as possible. This procedure yields the radial distribution function (RDF) which describes the probability to find an atom at a given distance from the excited one. The first and more intense peak of the FT is then filtered and inverse Fourier transformed to obtain the experimental $\chi_{\rm exp}(k)$ EXAFS contribution of the so selected coordination shells. For a fcc material such as Cu, $\chi_{\rm exp}(k)$ corresponds to the first near neighboring (NN) atoms (one shell) while for a bcc material such as W, the filtered EXAFS function $\chi_{\rm exp}(k)$ includes the contribution of the two first coordination shells (first NN's and second NN's).

The experimental filtered EXAFS function $\chi_{\rm exp}(k)$ was fitted to the theoretical one $\chi_{\rm th}(k)$ calculated from the widely reported formula[30]

$$k\chi_{\rm th}(k)=-S_0^2\sum_j N_j^*\frac{|f_j(\pi,k,R_j)|}{R_j^2}e^{-2R_j/\lambda(k)}e^{-2\sigma_j^2k^2}\times\sin[2kR_j+\phi_j(\pi,k,R_j)], \tag{8}$$

where R_j is the mean distance between the absorber and the jth shell, $|f_j(\pi,k,R_j)|$ is the backscattering amplitude for the jth neighboring atoms and $\phi_j(\pi,k,R_j)$ is the total phase shift. The backscattering parameters are R_j dependant to account for curvature effects of the ejected photoelectron wave function. The exponential decay factors are related to the mean free path $\lambda(k)$ of the ejected photoelectron and mean square relative displacement of the absorber-backscatter pair (Debye-Waller factor σ_j^2), respectively. The overall amplitude reduction factor S_0^2 accounts for many-body effects. For anisotropic systems, N_j^* is the effective polarization dependent coordination number defined as[31]

$$N_j^*=3\sum_{i=1}^{N_j}\cos^2\theta_{ij}, \tag{9}$$

$$N_j^*=(0.5+c)N_j+(1.5-3c)\sum_{i=1}^{N_j}\cos^2\theta_{ij}, \tag{10}$$

where θ_{ij} is the angle between the electric field vector $\mathbf{E}$ and the bond between the absorbing atom and the jth neighbor of the ith shell. Eq. (9) holds at the Cu K edge while Eq. (10) must be used at the W L_3 edge. The factor c appearing in Eq. (4) is the ratio of the radial dipole matrix elements M_{01} and M_{21} between the $2p$ ($l=1$) atomic wave function and the d ($l=2$) and s ($l=0$) final states.[32] It has been shown that the angular dependences of these two terms can be strongly different for noncubic materials.[20] However, this effect is much less pronounced for cubic or sightly tetragonal structures where the absorption cross section is isotropic.[33]

The theoretical EXAFS function $\chi_{\rm th}(k)$ calculated according to Eq. (8) was compared to the experimental one $\chi_{\rm exp}(k)$ by varying the parameters N_j, R_j, σ_j^2, and E_{0j} in order to minimize the variance V defined by

$$V=\frac{\sum_{i=1}^{n}[(k_i\chi_{\rm exp}(k_i)-k_i\chi_{\rm th}(k_i)]^2}{\sum_{i=1}^{n}[(k_i\chi_{\rm exp}(k_i)]^2} \tag{11}$$

for the n data points by using a simplex and/or gradient method implemented in the Michalowicz's software.[28] The number of independent points in the data N_{idp} is given by $N_{idp}=2\delta k\delta R/\pi+2$, where δR is the width of the selected peak of the FT's for inverse Fourier transformation and δk is defined by the energy range of the Kaiser window used to obtain the FT's. It results that the number of floating parameters during the fitting procedure is restricted to N_{idp} - 1. In the present case, the experimental available δk range was large enough to allow to keep a free degree of freedom during the fitting procedure at both Cu K ($N_{idp}=8$) and W L_3 (N_{idp} = 12) edges.

To obtain reliable informations from an EXAFS analysis, one is required to use confident backscattering parameters (amplitudes and phase shifts) since the results are strongly dependant on them. In the present work, we have adopted the following scheme. For Cu K analysis, we use backscattering amplitude and phase shift extracted from the data collected on a pure bulk Cu reference sample in the same experimental conditions as those used for probing multilayers (same temperature, same device). This bulk reference sample was at first mechanically and electrochemically polished and then annealed at 600 °C in vacuum over 6 h. For fcc Cu, the first peak of the FT is only related to the first coordination shell (twelve NN's), a particularity that allows one to quite easily obtain the backscattering parameters from Eq. (8) restricted to the first shell once the first NN's distance R_1 and Debye-Waller (DW) factor σ_1 are known. In the present case, we have used the value $R_1=2.556$ Å, as deduced from the crystallographic lattice parameter $a_{Cu}=3.615$ Å, while the DW factor was fixed to $\sigma_1=0.057$ Å, a value that has been experimentally deduced from measurements[34] performed at the liquid nitrogen temperature as in our experiments and that is supported by theoretical models.[35] The photoelectron mean free path $\lambda(k)$ has been modeled by the expression[27]

$$\lambda(k)=\frac{1}{\Gamma}\left[k+\left(\frac{\eta}{k}\right)^4\right] \quad (12)$$

with $\Gamma=1$ Å^{-2} and $\eta=3.1$ Å$^{-5/4}$, two parameters which are kept fixed during the Cu K edge simulations presented below. Such a procedure cannot be use for a bcc structure as that of tungsten since the first peak of the RDF involves the contributions of the two first coordination shells (that include eight and six atoms, respectively). Therefore, we have used the following method. First, we perform a purely theoretical calculation using the *ab initio* FEFF code[36] at the W L_3 edge taking as lattice parameter its usually quoted crystallographic value ($a=3.165$ Å). In that calculation, we use the analytical model of Hedin-Lundquist for exchange to obtain the photoelectron mean free path $\lambda(k)$ that was used for all simulations performed at this edge. In a second step, the so obtained theoretical backscattering parameters (amplitudes and phase shifts) corresponding to the two first coordination shells where used as input parameters to fit the two first shells filtered EXAFS data related to a pure W reference sample. The best fit results are displayed in Fig. 1, the corresponding set of structural parameters being gathered in Table I. The overall agreement between the experimental and

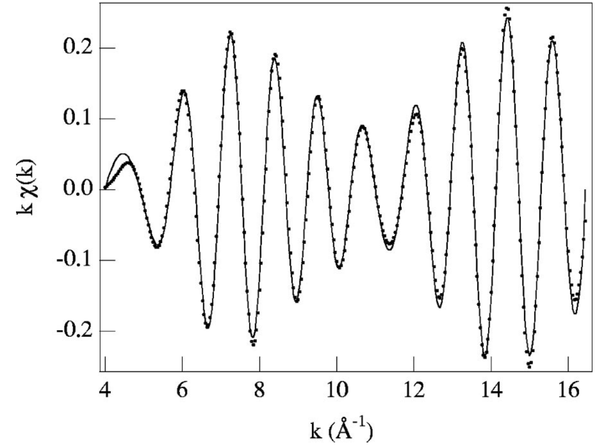

FIG. 1. Bulk tungsten experimental (symbols) and fitted (full line) filtered $k\chi(k)$ EXAFS spectra.

reconstructed filtered EXAFS signals is quite good. The distances are found to be slightly shorter than those deduced from crystallography ($R_1=2.741$ Å , $R_2=a=3.165$ Å) but close to them within the error bars. The value we obtain for the overall reduction factor S_0^2 is quite comparable with those usually found when using the FEFF code for analyzing EXAFS data.[37] This parameter was fixed to the value so obtained (0.77) during the fitting procedure used to analyze all W L_3 edge spectra of the W/Cu multilayers.

III. RESULTS AND DISCUSSION

A. Structure of the Cu/W multilayer before and after ion irradiation: short overview

The experimental $k\ \chi(k)$ EXAFS spectra recorded at the W L_3 edge of the as-deposited Cu/W multilayer for both grazing (parallel polarization) and normal (almost perpendicular polarization) incidences are presented in Fig. 2. In the same figure is also plotted the spectrum recorded at the grazing incidence for the ion beam irradiated multilayer at the same edge. Figure 3 shows the corresponding FT's and the related two first shells filtered $k\ \chi(k)$ EXAFS curves are displayed in Fig. 4. The examination of this set of curves calls for two remarks. The first one concerns the unirradiated sample spectra: differences between the W structure in the plane of growth and in the growth direction are revealed by comparing the FT's of the spectra recorded with the surface parallel and nearly perpendicular to the polarization direction of the x-ray beam. This behavior is also clearly observed on the related $k\ \chi(k)$ filtered EXAFS curves (Fig. 4) which amplitudes have a very different shape at high k (beyond 12

TABLE I. Structural parameters deduced from the least squares fit of the two first shells of NN's for bulk tungsten (k range: 4–16.5 Å^{-1}; $S_0^2=0.77\pm0.02$; $V=9.3\times10^{-3}$).

	N	Distance (Å)	σ (Å)
First shell	8	2.730±0.007	4.1 (±0.5)×10^{-2}
Second shell	6	3.160±0.007	4.9 (±0.5)×10^{-2}

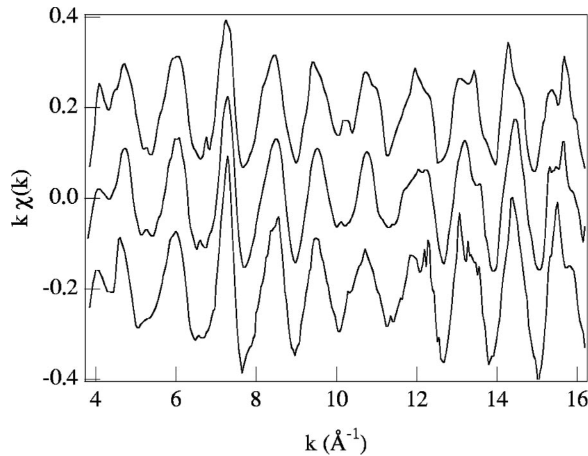

FIG. 2. $k\chi(k)$ EXAFS spectra recorded at the W L_3 edge of the as-deposited (top: parallel polarization ; middle: perpendicular polarization) and irradiated (bottom) Cu/W multilayers.

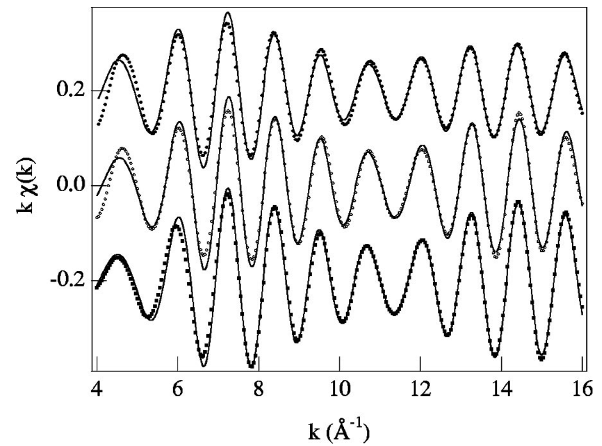

FIG. 4. Experimental (symbols) and fitted (full lines) filtered $k\chi(k)$ EXAFS spectra recorded at the W L_3 edge of the as-deposited (top: parallel polarization; middle: perpendicular polarization) and irradiated (bottom) Cu/W multilayers.

$Å^{-1}$) compared to that of the pure tungsten reference (Fig. 1), especially for the parallel polarization. The second one is related to the ion beam irradiated sample: its spectrum looks more similar to the reference one (Fig. 1) save for an overall amplitude reduction, an effect that may be related to an increased disorder compared to the bulk reference. These simple statements show that the irradiation is able to induce relaxation effects into the W sublayers of the multilayer, whose initial structure is much different than that pure bcc tungsten. Such a behavior does not seem to hold in Cu layers as it can be shown in Fig. 5. Indeed these Cu *K* EXAFS spectra, recorded at grazing incidence, look for the eyes very close each from the other. The related FT's shown in Fig. 6 also evidenced that the irradiation induces an overall enhancement of the magnitude of the EXAFS signal related to an improvement of the cristallinity of the Cu sublayers without reaching, however, that of bulk Cu. Furthermore, one can note that the Cu structure is really fcc up to ~7.5 Å (six shells) because both multilayers' FT's are homothetic to the bulk one up to that distance.

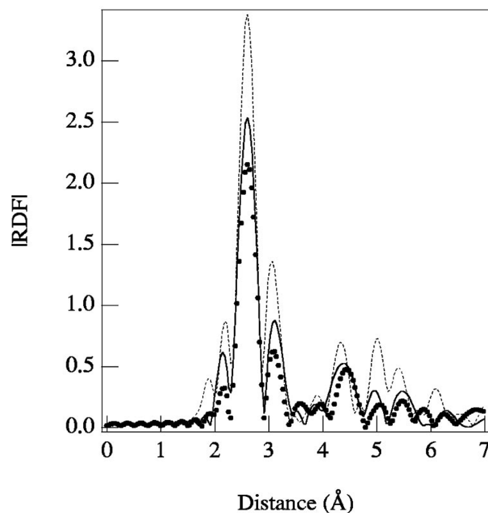

FIG. 3. Fourier transforms of the EXAFS spectra recorded at the W L_3 edge of as-deposited (symbols: parallel polarization, full line: perpendicular polarization) and irradiated (dotted line) Cu/W multilayers.

XRD θ-2θ scans in the angular range corresponding to W (110) and Cu (111) Bragg's reflections are shown in Fig. 7 for both the as-deposited and ion beam irradiated Cu/W multilayers. These experimental spectra do not exhibit the usual features of multilayers' diffraction profile: superlattice diffraction peaks arising from the periodicity of the multilayer. That comes from the fact that the coherence length is smaller or close to the period Λ. In such cases it does not exist a periodic modulation of the crystalline structure inside diffracting grains, and so the XRD spectra do not exhibit the satellite peaks characteristic of superlattices. The reflection peaks observed in the whole 2θ range have been assigned to x-ray scattering by the dense atomic planes of both components of the multilayer [(110) for bcc W, (111) for fcc Cu]. Concerning the as-deposited multilayer, a large lattice expansion of the W layers is observed since the lattice spacing distance d_W^{110} deduced from the (110) W reflection is greater

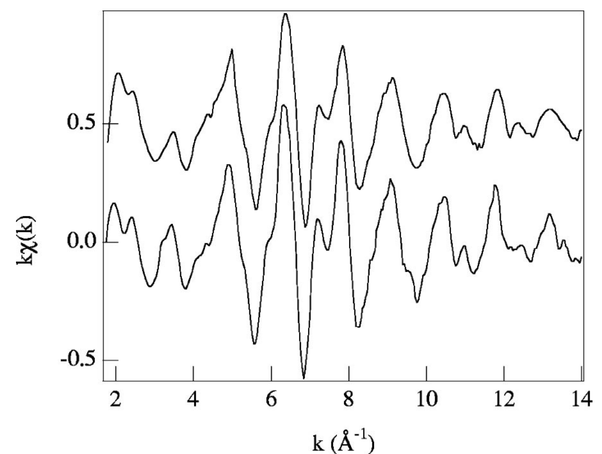

FIG. 5. $k\chi(k)$ EXAFS spectra recorded at the Cu *K* edge of the as-deposited (top) and irradiated (bottom) Cu/W multilayers.

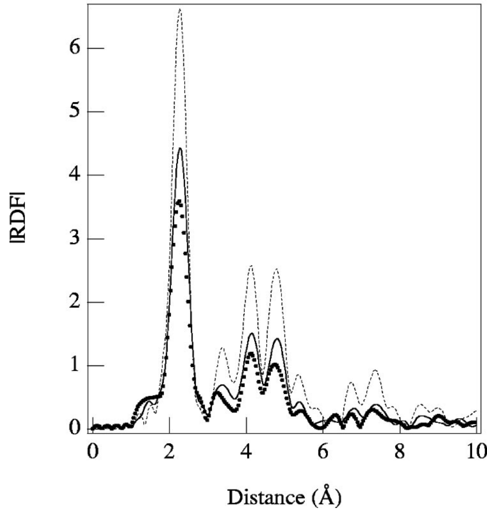

FIG. 6. Fourier transforms of the EXAFS spectra recorded at the Cu K edge of as-deposited (symbols), irradiated (full line) Cu/W multilayers, and bulk Cu (dotted line).

($d_{\mathrm{W}}^{110}=2.267$ Å) than the bulk one ($d_{\mathrm{W\,(bulk)}}^{110}=2.238$ Å). After irradiation with krypton ions at the fluence of 10^{13} ions/cm^2, we observe a visible shift of the W(110) reflection towards lower angles. This could clearly be related to an ion induced strain-stress relaxation effect as was already evidenced in Cu/W multilayers with a shorter periodicity length.[38] Thus it appears that, due to the Poisson effect, the out-of-plane lattice expansion of the bcc tungsten stacking can be attributed, at least partially, to in-plane compressive stresses. In turn, the measured interplanar distance ($d_{\mathrm{Cu}}^{111}=2.093$ Å) of the (111) Cu layers appears to be very close to that of bulk copper (2.087 Å).

To summarize, the simple qualitative analysis from the XRD spectra recorded with the wave vector in the growth direction gives evidence for the presence of strong elastic strains in the as-deposited tungsten layers of the Cu/W multilayer. EXAFS data are sensitive to the presence of such lattice strains and to relaxation effects induced after ion irradiation. To go beyond this qualitative description, it is necessary to perform simulations that will be discussed hereafter. Therefore, the issue is whether the average local atomic environment described by the respective in-plane and out-of plane distances can be sufficiently reliable to obtain a complete determination of the strain-stress state of the elemental layers. For this purpose, by modeling the elastic response of the material, a comparative study of stress and unstrained lattice parameters deduced from the EXAFS data with those obtained from the usual x-ray scattering method must be carried out.

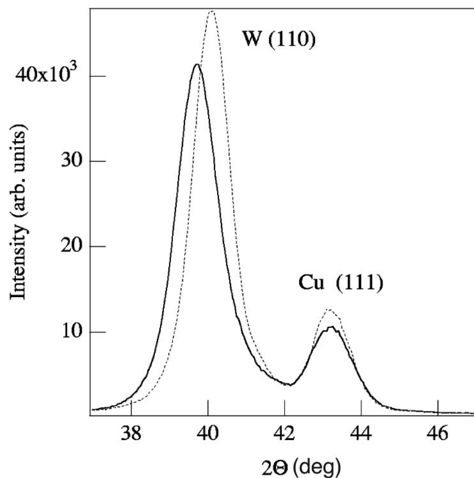

FIG. 7. XRD spectra of the as-deposited (full line) and irradiated (dotted line) Cu/W multilayers.

TABLE II. Structural parameters deduced at the W L_3 edge from the least squares fit of the two first shells of NN's for the as-deposited Cu/W multilayer for the parallel polarization (k range: 3.9–16 Å^{-1}; $V=2.3\times10^{-2}$). In-plane (N^{in}) and out-of-plane (N^{out}) effective coordination numbers N^* are determined according to Eq. (10) using a ratio $c=0.2$ (see text).

	N^*	Distance (Å)	σ (Å)
First shell	4.8^{in}	2.701 ± 0.007	$7.1\ (\pm0.6)\times10^{-2}$
	3.2^{out}	2.743 ± 0.007	$4.5(\pm0.6)\times10^{-2}$
Second shell	2^{in}	3.110 ± 0.007	$11(\pm1)\times10^{-2}$
	4^{out}	3.155 ± 0.007	$6.6\ (\pm0.6)\times10^{-2}$

B. As-deposited multilayer: strain-stress analysis

1. EXAFS data analysis

Tungsten sublayers. The effective coordination numbers N_j^* have been fixed according to Eq. (10). The ratio c has been calculated theoretically:[39] it is found to be approximately 0.2 for atomic numbers $Z>20$ and relatively independent of k. This value is in agreement with the one experimentally determined by Held and Stern[32] at the W L_3 edge on anisotropic $\mathrm{WSe_3}$. Taking this value, one obtains the in and out-of-plane effective coordination numbers reported in Tables II and III for the parallel and perpendicular polarization, respectively. Each shell splits in two components and thus it needs to handle a model looking like a four shells model. Therefore, we adjust ten parameters : four distances, four DW factors and two energy shifts E_0 to correct the error in FEFF's Fermi level estimate [8.0(±0.3) eV and 6.4 (±0.3) eV for the first and second shell, respectively]. The

TABLE III. Structural parameters deduced at the W L_3 edge from the least squares fit of the two first shells of NN's for the as-deposited Cu/W multilayer for the perpendicular polarization (k range: 3.9–16 Å^{-1}; $V=1.6\times10^{-2}$). In-plane (N^{in}) and out-of-plane (N^{out}) effective coordination numbers N^* are determined according to Eq. (10) using a ratio $c=0.2$ (see text).

	N^*	Distance (Å)	σ (Å)
First shell	2.8^{in}	2.709 ± 0.007	$6.1(\pm0.6)\times10^{-2}$
	5.2^{out}	2.731 ± 0.007	$5.0(\pm0.6)\times10^{-2}$
Second shell	1.4^{in}	3.110 ± 0.007	$11\ (\pm1)\times10^{-2}$
	4.6^{out}	3.151 ± 0.007	$5.7(\pm0.6)\times10^{-2}$

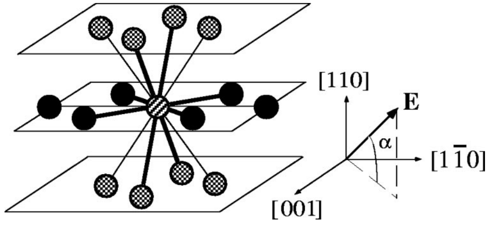

FIG. 8. Two first-nearest-neighbors shells of a tungsten atom. Each absorber (cross hatched circle) has six NN's in its (110) plane (black circles) and eight other NN's out-of-plane (gray circles). Thick lines: first NN bonds, thin lines: second NN bonds. Parallel polarization: $\alpha = 0°$; perpendicular polarization: $\alpha \approx 77°$.

results of fitted curves are shown in Fig. 3 for both polarizations while the corresponding structural parameters are summarized in Table II (parallel polarization) and Table III (perpendicular polarization). Excepted in the range 6–7 $Å^{-1}$ where the amplitude of the reconstructed spectra does not match the experimental data perfectly, the results so obtained can be considered as acceptable. In particular, the anomalous shape of the filtered EXAFS at high k previously mentioned for the parallel polarization is fairly reproduced. We can emphasize that, within the uncertainties, the deduced structural parameters are equal for both polarization geometries. From their values, we can assess that in-plane atoms are located at significantly shorter distances than in the bulk tungsten (see Table I), while the out-of-planes atoms (that are *not* located along the perpendicular direction, see Fig. 8) are observed at distances close to those found for the bulk tungsten reference. This is consistent with the XRD observations quoted above and it implies that (110) W planes are submitted to a compressive stress. However, this compressive state of the W layers is accompanied by an increased atomic disorder within the (110) planes since the in-plane DW factors are much more important than the out-of-plane ones, especially for second NN's. This last fact appears to be surprising at first glance. Indeed, due to the presence of strong in-plane compressive stresses in the W layers, one should expect to observe reduced thermal vibrations for in-plane bondings compared to out-of-plane ones. Nevertheless, since EXAFS spectra were recorded at liquid nitrogen temperature, static atomic disorder dominates the measured DW factors. Therefore, any in-plane lattice distortion of the bcc lattice would involve an apparent increase of the DW factors. In this context, it is well known[40,41] that epitaxy occurs following the Nishiyama-Wassermann orientation relationship between the two bcc and fcc lattices constituting the Cu/W multilayers. Such an atomic arrangement, generating strain anisotropy between the two in-plane directions, would imply a difference between DW factors for both directions that may be responsible of the anomalous DW factors we obtain for in-plane atoms.

Copper sublayers. The data at the Cu K edge data have been only recorded at the grazing incidence (parallel polarization). In such a case, according to Eq. (9), one has to consider the contributions of in-plane and out-of-plane first NN's separately. Therefore, theoretically five parameters are required to adjust the simulated spectrum to the experimental

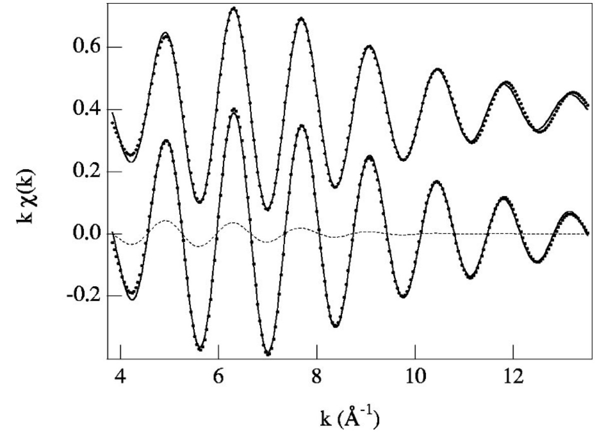

FIG. 9. Experimental (symbols) and fitted (full lines) filtered $k\chi(k)$ EXAFS spectra recorded at the Cu K edge of the as-deposited (top) and irradiated (bottom) Cu/W multilayers. Dashed line: contribution of out-of-plane atoms for the irradiated multilayer (see text).

one: two distances, two DW factors and an energy shift E_0 (that was found to be close to 0 eV). However, in the case of a fcc structure grown in the (111) direction, the contribution to EXAFS from up and down planes is small for the parallel polarization (nine effective in-plane bonds versus three effective out-of-plane bonds). The EXAFS spectra recorded with parallel polarization are thus mostly sensitive to in-plane atoms. In fact, it turns out that the fitting procedure is insensitive to out-of-plane atoms: one gets unphysical DW factors for these atoms (greater than 0.3Å) and thus to include their contribution into the reconstructed EXAFS signal is meaningless. Indeed, considering only in-plane atoms, one obtains an acceptable fit of the experimental data as it can be observed in Fig. 9, the corresponding parameters being reported in Table IV. Even if the first NN distance can be considered to be, within the error bars, equal to that of pure copper, it seems that the Cu lattice is slightly expanded in plane since it will correspond to an in-plane lattice parameter $a_{\parallel} = 3.622$ Å. Noting that XRD is in the present case only sensitive to the direction of growth that is orthogonal to the one probed by EXAFS, from the XRD spacing value quoted before $d_{\mathrm{Cu}}^{111} = 2.093$ Å, one obtains $a_{\perp} = 3.625$ Å. These two values can be considered, owing to the experimental uncertainties, as equal and thus the Cu lattice expanded by ~ 0.01 Å, but it is important to note that the Cu sublayers structure appears isotropic. The origin of such a slight Cu lattice expansion may be due to the numerous defects (dislocations, extended or point defects such as interstitials) that are intro-

TABLE IV. Structural parameters deduced at the Cu K edge from the least squares fit of the first shell of NN's for the as-prepared Cu/W multilayer (k range: 3.7–13.7 $Å^{-1}$; $V = 5.8 \times 10^{-3}$). The in-plane (N^{in}) effective coordination number N^* is determined according to Eq. (9).

N^*	Distance (Å)	σ (Å)
9^{in}	2.561 ± 0.008	$7.1\ (\pm 0.5) \times 10^{-2}$

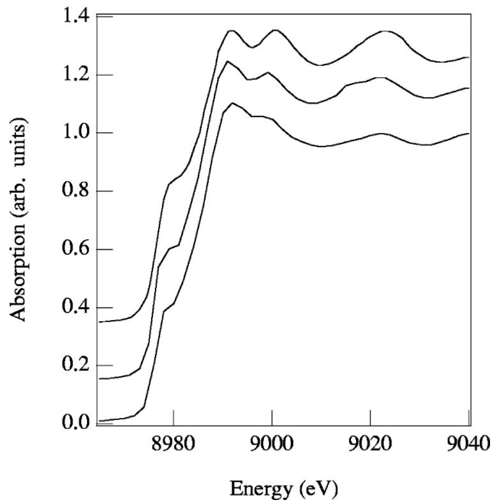

FIG. 10. Cu K edge XANES spectra of the as-deposited (bottom), irradiated (middle) Cu/W multilayers and bulk Cu (top) for comparison.

duced by the relaxation of the Cu layers during growth. For example, the amount of argon atoms incorporated into the superlattice during the elaboration process is of about 0.7%, while the presence of extended defects (stacking faults or twins) inside Cu layers is evidenced from HRTEM observations.[42] These defects can account for the quite high DW factors we found, but they can be also at the origin of what that makes the EXAFS signal insensitive to the contribution of out-of-plane atoms. Furthermore the presence of extended defects inside Cu sublayers would imply a modification of the copper electronic structure that is evidenced from the examination of the Cu K XANES (x-ray absorption near edge structure) spectra shown in Fig. 10: one notes an inversion of the two peaks at the top of the edge for the as-deposited multilayer compared to the bulk.

To end, we must mention the particularities of the detection technique used here that can be a possible cause for the lack of sensitivity we observe for probing out-of-plane atoms at the Cu K edge in the parallel geometry. Indeed, it has been demonstrated[43] that the total-electron-yield (TEY) signal is very sensitive to the nature of the probed atomic species through the energy dependence of the corresponding escaping electrons (KLL Auger, secondary electrons, etc.). Furthermore, it has been reported unequivocal evidence for "self-absorption" distortions intrinsic to TEY detection at grazing incidence.[44] In our case, the incidence angle used for the parallel polarization is high enough (13°) so that "self-absorption" will be expected to remain limited. This is confirmed by the fact that such an effect is not observed in tungsten sublayers where the use of coordination numbers of a bcc structure yields good fits of the experimental data.

2. Elasticity analysis

EXAFS probes the local symmetry of the absorbing atom through a set of atomic distances analysis corresponding to different first near neighboring atomic shells. Thus, similarly to conventional XRD strain measurements, EXAFS potentially allows one to determine the internal stress state of the superlattices constituents. Indeed for a strained layer, the directions belonging to the same shell are no longer equivalent. The strain analysis can simply be extended to the EXAFS data by substituting the information on lattice spacings for a bcc tungsten structure from Eq. (5) by the atomic distances R_i. The EXAFS analysis of the first shells reported above yields two in-plane distances ($\psi=90°$) and two out-of-plane distances related to first and second NN bondings corresponding, respectively, to the two different directions $\psi=35.26°$ and 45°. By considering the local atomic environment of W atoms shown in Fig. 8 and by referring to Eq. (5), save, however, for in-plane second NN's bonds, a weak sensitivity of the different bonding shells to a nonequal biaxial stress state is expected. In addition to the inherent weak accuracy of the EXAFS analysis, the contribution of the $(\sigma_{11}-\sigma_{22})$ term in Eq. (5) is expected to be weak for both out-of-plane and in-plane first NN's distances by accounting for the weak values of both the elastic coefficient and the $\cos 2\phi \sin^2\psi$ factor in the corresponding bonding directions. Thus, the four in-plane first NN's bondings are shared at quasisymmetrical directions relatively to the main twofold axis of the (110) planes and consequently the atomic in-plane distances will be very close to the in-plane average lattice parameter. On the other hand, to observe an in-plane second NN's distance ($\phi=90°$ and $\psi=90°$) nonconsistent with the first NN's one is able to indicate some anisotropy between the in-plane stress components. The averaged lattice parameters deduced from the determination versus $\sin^2\psi$ of the in-plane and out-of plane first and second NN's distances for both parallel and perpendicular polarizations are reported in Fig. 11(a). First, we can remark the relatively good alignment of the measurements belonging to the in-plane first NN's and out-of-plane first and second NN's, while the slope clearly evidences that the stress is compressive. On the other hand, the in-plane second NN's bonding distance appears smaller than expected from this overall behavior. As-above emphasized, such a large strain for bonds belonging to the [001] direction can be ascribed to a possible anisotropy of the stress state in the [110] planes of the tungsten layers. Therefore it could indicate that compressive stresses are stronger in this crystallographic direction. As quoted previously, such an hypothesis is quite compatible with the Nishiyama-Wassermann orientation relationship between the two lattices. Nevertheless, accounting for the weak yield of these bonds in the EXAFS analysis, additional data are required to support this coherency effect. The analysis of the out-of-plane and in-plane NN's atomic distances, and more precisely of their ψ dependence using Eq. (5), can allow one to extract the two main unknowns that are the average stress $\bar{\sigma}$ and the free-stress lattice parameter a_0. If we assume the elastic compliance constants to be equal to those of the bulk ($s_{11}=2.49\ \mathrm{TPa}^{-1}$; $s_{12}=-0.7\ \mathrm{TPa}^{-1}$; $s_{44}=6.35\ \mathrm{TPa}^{-1}$),[45] a stress value $\bar{\sigma}\sim-5.6\ (\pm1.5)$ GPa and a free-stress lattice parameter $a_0\sim3.156$ Å are deduced from the best fit to the W sublayers data. The linear a versus -$\sin^2\psi$ dependence gives an extrapolated value at $\psi=0$ yielding to the lattice parameter in the direction of growth $a_\perp=3.182$ Å, a value smaller than the one (3.202 Å) deduced from x-ray measure-

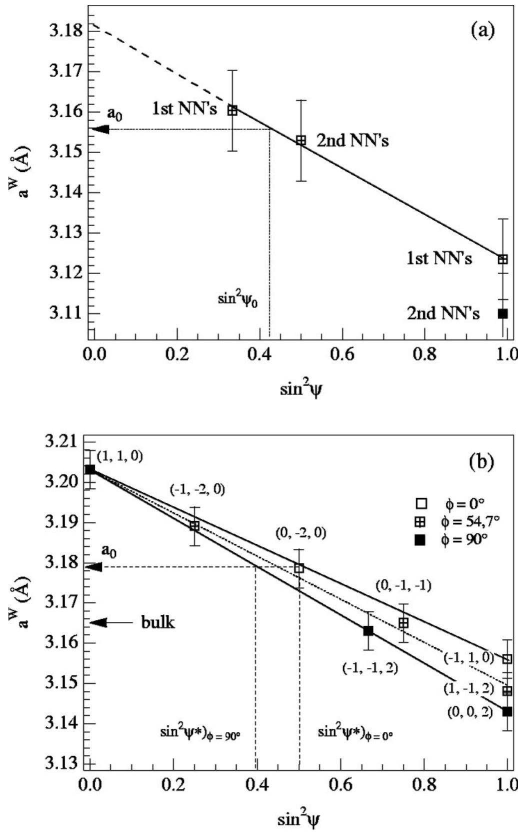

FIG. 11. Lattice parameters of tungsten layers determined from NN's EXAFS distances (a) and XRD interplanar spacings (b) at different ϕ angles and the corresponding linear fits according to Eq. (5). The EXAFS second in-plane NN's [(a) black symbol] are excluded from the fit (see text).

ments. In addition, the free-stress lattice parameter appears to be also slightly smaller than the pure bulk tungsten one, it is, however, approximately consistent with the one of the W bulk reference obtained from the EXAFS analysis. It is here difficult to define standard errors, the number of parameters being indeed very comparable to the number of points of measurement. From Eq. (5), one can, however, note that the accuracy of the stress value depends of course on that of the distances deduced from the EXAFS measurements, but also on the value chosen for the compliance constant s_{44}. On the opposite, the accuracy on the determination of the free-stress lattice parameter from the free-stress direction is weakly dependent on the elastic constant values. The error given above for the averaged biaxial stress $\bar{\sigma}$ reflects mainly the dispersion of the data deduced from the analysis performed for the two polarizations.

The question of the reliability to use the local atomic distances obtained from the WL_3 edge EXAFS data in term of elasticity to analyze strains is of course raised. To get some insight about that point, we have carry out a detailed XRD study of the same sample. It is worth to remind that the Cu/W superlattices studied here are fiber-textured multilayers. Therefore, the measurements of the lattice spacings have been performed according to the ideal crystallite group method described in the Sec. II C. Only reflection lines giving a good signal to background scattered intensity ratio have been kept here and we systematically perform measurements for positive and negative ψ values. The lattice parameter values deduced from the lattice spacing measurements related to different $\{hkl\}$ planes at various selected (ϕ,ψ) poles, and distributed according to three azimuthal directions ($\phi=0$, 54 and 90°), are reported in Fig. 11(b). Both the alignment of the different measurements corresponding to a same ϕ angle and the extrapolation towards a common value equal to the (110) lattice parameter (determined with the scattering vector perpendicular to the surface sample) support the fact that it exists a nonequal biaxial compressive stress state in W sublayers. It indicates the presence of coherency stresses between the two bcc and fcc constituents. So, the principal stresses σ_{11} and σ_{22} along the directions $[\bar{1}10]$ and $[001]$ of the sample reference frame appear to be such that $|\sigma_{11}|>|\sigma_{22}|$ implying an epitaxial atomic arrangement with a larger strain in the $[001]_{\mathrm{bcc}}$ direction assumed to be parallel to the $[1\bar{1}0]_{\mathrm{fcc}}$ direction of the fcc lattice according to the Nishiyama-Wasserman orientation relationship. The three unknown parameters (the free-stress lattice parameter a_0, the stresses σ_{11} and σ_{22}) can be easily deduced from the slopes of the curves a versus $\sin^2\psi$ and from the stress-free directions ψ^*. One obtains $a_0\sim3.178$ Å, $\sigma_{11}=-4.7$ GPa, and $\sigma_{22}=-6.0$ GPa. Thus, an average in-plane stress $\bar{\sigma}$ of -5.3 (±0.3) GPa in the tungsten layers is estimated from this analysis, a value in a quite good agreement with the one deduced from the analysis of the EXAFS data quoted above.

However, the stress-free lattice parameter appears to be significantly larger than the known bulk value. Such an effect has already been mentioned previously in W films elaborated using the same sputtering method.[46] The influence of point defects such as self-interstitial atoms in these very thin layers grown far from equilibrium has often been evoked. Although the atomic concentration in trapped argon atoms as determined from EDX measurements is less than 1%, their presence in substitutional sites may also significantly contribute to the observed crystalline lattice expansion. With the sputtering conditions used here for depositing the multilayer (low working pressure and strong ion-beam energy), it is worth emphasizing that the growing crystalline film experiences an autobombardment in the range from ten to hundreds of electronvolts. In good agreement with the previous model of "atomic peening,"[47] recent simulations[48] have demonstrated that under such irradiation conditions, e.g., for near threshold events, a lot of interstitials are produced far from the surface by long-range replacement sequences occurring into the crystalline target. Nevertheless, it remains to understand why such a specific contribution to the signal is not detected during the EXAFS analysis, a point that will be addressed later.

In principle, a similar analysis can be carried out for a (111) fcc stacking submitted to internal stresses. As discussed before, the analysis of both the XRD and EXAFS signals really allow us to assess that the copper lattice is unstrained and free of stress. Furthermore, due to the too weak x-ray scattering power of copper atoms, no reliable

strain analysis using the XRD method could be performed in these polycrystalline copper layers.

3. Total stress state of as-sputtered Cu/W multilayers

The lattice parameter measurements, combined with the elasticity analysis deduced from two independent methods, have allowed us to determine the strain and stress state within each element constituting the multilayer. Another source of stress that is important to consider in multilayered films is the interface stresses.[10,49] For the here studied Cu/W multilayer, taking an interface stress value equal at the most to 2 J/m^2 and a layer thickness of 10 nm, the interfacial component is weak: it will not exceed 0.2 GPa and so its contribution to the total stress state can be safely neglected. Thus, a strong stress gradient with alternate free of stress copper layers and compressive stress in tungsten ones is developed into the Cu/W multilayer leading to an overall compressive state. Using a method similar to the one outlined by Bain *et al.*,[8] the total stress can be deconvoluted into coherency stresses and a substrate-interaction stress. The coherency stresses are assumed to induce equal and opposite forces into the layers, while the substrate interaction stresses are the result of a balance between the forces existing into the whole film and into the substrate. The stress analysis of the tungsten layers presents some evidence for the presence of coherency stresses since we observe a dependence of the stress magnitude with the probed crystallographic direction. In such a heteroepitaxial system, this in-plane anisotropy is ascribed to the formation of coincidence structures. The mechanical equilibrium between forces therefore requires that corresponding tensile coherency stresses exert an equal and opposite traction inside individual copper layers. Thus, the absence of any residual elastic strain into copper layers appears at first glance surprising. That can nevertheless occur if a large compressive substrate-interaction stress, generated during the film growth and involving atomic rearrangements, counterbalances the tensile strain-stress existing into the copper layers.[50] Since the intrinsic substrate-interaction stress σ^{SI} acts equally into the whole film, one can write the average total stress for each constituent as

$$\bar{\sigma}_{Cu}^{tot}=\bar{\sigma}_{Cu}^{coh}+\sigma^{SI} \quad \text{and} \quad \bar{\sigma}_{W}^{tot}=\bar{\sigma}_{W}^{coh}+\sigma^{SI} \tag{13}$$

with

$$\bar{\sigma}_{Cu}^{coh}t_{Cu}=-\bar{\sigma}_{W}^{coh}t_{W}, \tag{14}$$

where $\bar{\sigma}_{Cu}^{coh}$ and $\bar{\sigma}_{W}^{coh}$ are the average of the principal coherency stresses into copper and tungsten layers; t_{Cu} and t_W being their respective thicknesses. According to Eqs. (13),(14) and using as values for $\bar{\sigma}_{Cu}^{tot}$ and $\bar{\sigma}_{W}^{tot}$ those deduced from the experimental XRD data quoted above, we find a compressive substrate-interaction stress $\sigma^{SI}\approx-2.8$ GPa and for the coherency tensile and compressive stresses into the copper and tungsten layers: $\bar{\sigma}_{Cu}^{coh}\approx 2.8$ GPa and $\bar{\sigma}_{W}^{coh}\approx-2.5$ GPa. Such high substrate-interaction compressive stresses are commonly observed in sputtered films grown at low pressures. It would result from the damage created by atoms with energy higher or close to the damage threshold. A considerable number of interstitials are produced inside the first atomic planes whereas vacancies, formed only close to the surface, are eliminated by spontaneous recombination with adatoms.[48] Taking into account this additional balistic mechanism, the reduction of the elastic energy density in the growing layer leads to a different mechanical stress state in the heteroepitaxial system. As a result, atomic rearrangements generate an overall substrate-interaction stress which leads to a nearly complete stress relaxation of copper layers and, simultaneously, to an enhancement of the compressive state of the tungsten layers. One can think that the high atomic disorder evidenced from the EXAFS analysis inside the copper layers, on the one hand, and the strong compressive stress observed in the tungsten layers, on the other hand, could support this scheme. Moreover, the expansion of the free-stress lattice parameter determined by x-ray measurements, attributed to recoil implanted atoms, would then be directly correlated to the overall compressive substrate-interaction stress. Finally, the magnitude of the average compressive stress into tungsten within these Cu/W multilayers is worth noting. Obtaining such stresses in thin layers, which are considerably higher than the bulk tungsten yield stress (which is in the MPa range), gives rise to several hypotheses. Size effect and yield strength for dislocation glide[51,52] are usually put forward. In addition, the extremely high point-defect density generated inside these thin films, able to reduce stiffness, can also be evoked as a source for generating such a high strain level.

TABLE V. Structural parameters deduced at the W L_3 edge assuming an unstrained bcc structure for the irradiated Cu/W multilayer (k range 3.9–16 Å^{-1}; $V=1.9\times10^{-2}$).

	N	Distance (Å)	σ (Å)
First shell	8	2.725 ± 0.007	$5.1\ (\pm0.5)\times10^{-2}$
Second shell	6	3.152 ± 0.007	$6.1\ (\pm0.5)\times10^{-2}$

C. Ion induced stress-strain relaxation

1. EXAFS data analysis

Tungsten sublayers. After irradiation with 10^{13} Kr/cm^2, two models were used to simulate the W L_3 edge data related to the ion beam irradiated Cu/W multilayer. From the similarities of the filtered EXAFS with the one related to pure tungsten noted previously, we use at first a simple bcc model (two shells), a scheme that appears sufficient to reproduce the experimental data with a set of structural parameters given in Table V. The distances are in that case found to be very close to those obtained for pure tungsten (Table I), a result consistent with the XRD data obtained for that sample (Fig. 7) since one observes a shift of the W (110) Bragg's reflection towards the angular position corresponding to pure tungsten. Nevertheless, the lattice parameter deduced from XRD (3.18 Å) appears higher than for the bulk and the EXAFS distances shorter than the reference ones, so that one can think that the W structure is still strained. Thus, we perform a second fit of the EXAFS data that takes into account the fact that the related W L_3 spectrum was recorded in

TABLE VI. Structural parameters deduced at the W L_3 edge from the least squares fit of the two first shells of NN's for the irradiated Cu/W multilayer for the parallel polarization (k range 3.9–16 Å^{-1}; $V=9.4\times10^{-3}$). In-plane ($N^{\rm in}$) and out-of-plane ($N^{\rm out}$) effective coordination numbers N^* are determined according to Eq. (10) using a ratio $c=0.2$ (see text).

	N^*	Distance (Å)	σ (Å)
First shell	$4.8^{\rm in}$	2.721 ± 0.007	$5.5\ (\pm0.6)\times10^{-2}$
	$3.2^{\rm out}$	2.730 ± 0.007	$4.6\ (\pm0.6)\times10^{-2}$
Second shell	$2^{\rm in}$	3.137 ± 0.007	$9.4\ (\pm0.6)\times10^{-2}$
	$4^{\rm out}$	3.153 ± 0.007	$4.7\ (\pm0.6)\times10^{-2}$

parallel geometry. According to Eq. (10), each shell splits into an in-plane and out-of-plane component, and using the same procedure as was done for the as-deposited sample, we obtain a fit whose factor merit is two times better than the two-shell model one. The result is displayed in Fig. 4 and the corresponding structural parameters are summarized in Table VI. Compared to the as-deposited case, we observe a strong reduction of the splitting between the in- and out-of-plane atoms for both first and second NN's. Thus both schemes evidence that stress relief is induced in the W layers after Kr ion irradiation at a fluence lower than 10^{13} ions cm^{-2} corresponding to a dose of only 0.04 dpa. However, the more statistically significant second fit also clearly shows that a fully relaxed stress state is not achieved at that fluence.

Copper sublayers. Concerning the Cu K edge data (grazing incidence), we fit the experimental filtered spectrum in the same way as it was done for the as-deposited multilayer. Looking at the results (Fig. 6 and Table VII), we do not observe any evolution of the distances inside Cu layers after ion irradiation except that we must now include the contribution of the out-of-plane atoms. Indeed, even if the related DW factor is quite high, their contribution to the measured signal is significant at low k values (see Fig. 6). To obtain equal in-plane and out-of-plane distances (that are furthermore, within the error bars, those of the unirradiated sample) yields to conclude that the ion irradiation does not modify the Cu structure that remains isotropic fcc: it only induces an improvement of the crystallinity of these layers evidenced by the reduction of the DW factors. However, one can note an evolution of the electronic structure of the Cu layers since the related XANES spectrum (Fig. 10) evolves towards that of pure Cu without reaching however the same electronic state since the intensities at the top of the edge jump are still reversed.

Quite generally, to observe an increase of the Cu first NN coordination number, weaker DW factors (one can note the same trend at the W L_3 edge) and a modification of the Cu K XANES structure indicates that the ion irradiation induces atomic rearrangements such that the positional disorder decreases in both Cu and W layers that evolve towards better defined fcc and bcc structures, respectively. This is also in agreement with the XRD results (Fig. 7) where one clearly observes a diminution of the width of the Bragg's reflections, especially concerning the (110) W peak.

TABLE VII. Structural parameters deduced at the Cu K edge from the least squares fit of the first shell of NN's for the irradiated Cu/W multilayer (k range 3.7–13.7 Å^{-1}; $V=2.6\times10^{-3}$). In-plane ($N^{\rm in}$) and out-of-plane ($N^{\rm out}$) effective coordination numbers N^* are determined according to Eq. (9).

N^*	Distance (Å)	σ (Å)
$9^{\rm in}$	2.565 ± 0.008	$6.2\ (\pm0.5)\times10^{-2}$
$3^{\rm out}$	2.566 ± 0.008	$14\ (\pm1)\times10^{-2}$

2. Elasticity analysis

The lattice parameters deduced from the determination of the in-plane and out-of plane first and second NN distances are reported versus $\sin^2\psi$ in Fig. 12(a). The stress into the tungsten layers deduced from an elasticity analysis relaxes towards a residual compressive state of approximately - 2.9 GPa, while the free-stress parameter appears unchanged or even slightly increased. The lattice parameters obtained from XRD measurements for different $\{hkl\}$ planes obtained at different selected (ψ,ϕ) poles are reported in Fig. 12(b). The lattice parameter obtained at $\psi=0$ (3.181 Å) is in excellent agreement with the one directly measured in the specular geometry. The negative value of the a versus $\sin^2\psi$ depen-

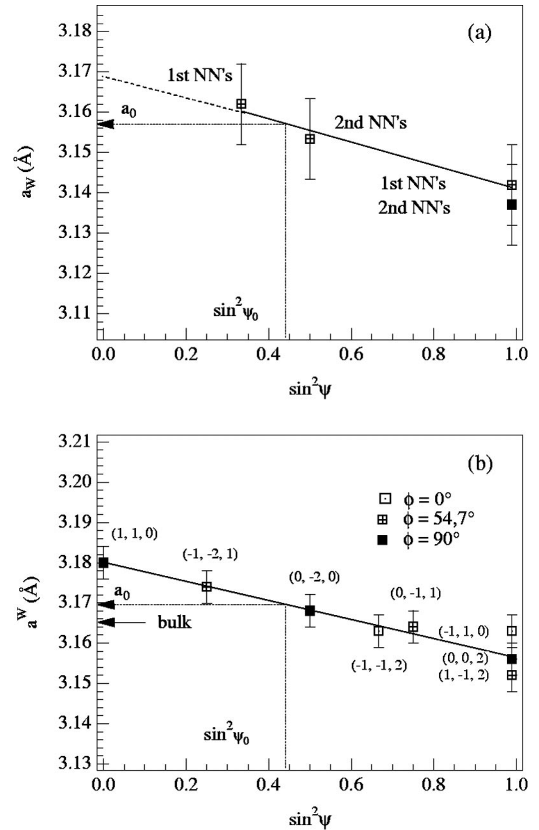

FIG. 12. Lattice parameters of tungsten layers determined from NN's EXAFS distances (a) and XRD interplanar spacings (b) at different ϕ angles after ion irradiation with 10^{13} Kr/cm^2 and the corresponding linear fits according to Eq. (5). The EXAFS second in-plane NN's [(a) black symbol] are excluded from the fit (see text).

dence indicates that tungsten layers still sustain residual compressive stress. Nevertheless at this relaxation stage, an equal biaxial stress state is reached since no clear ϕ dependence is observed on the scans. The stress analysis yields an average in-plane stress $\bar{\sigma}_{\mathrm{W}}^{\mathrm{tot}}$ of $-2.5(\pm 0.3)$ GPa and an unstrained parameter $a_0 \approx 3.169$ Å. Thus, after an ion fluence of 10^{13} Kr/cm^2 (corresponding to only 0.04 dpa), the stress is relaxed to about one half of its original value. It should be emphasized here that the magnitude of the residual compressive stress so obtained is quite consistent with the one deduced from the analysis of the EXAFS data. However, the lattice parameters determined from XRD measurements are again observed at slightly larger values than those deduced from the EXAFS analysis. Whereas no significant change is seen through the EXAFS analysis, a clear reduction of the free-stress lattice parameter ($\delta a_0 \sim -0.01$ Å) towards a value close to the bulk one is evidenced from XRD results. To explain this difference, one may at first consider alloying effects between the two different materials. Nevertheless, by referring to a previous work devoted to the study of ion induced mixing effects in this very immiscible Cu/W system,[53] ion beam mixing for such a low ion fluence is quite negligible. Secondly, considering the previously made hypothesis that the free-stress lattice parameter dilatation evidenced from XRD measurements into W layers comes from an out-of-equilibrium formation of interstitial atoms (either self-interstitials or trapped argon atoms), one can assume that the irradiation triggers their clustering or even their elimination at surface or interface sinks. Such a concomitant reduction of the stress-free parameter with the level of the compressive substrate-interaction stress in pure tungsten films has already been put forward.[46] One can therefore question if the observed discrepancy between XRD and EXAFS for the stress-free lattice parameter determination is not inherent to the method used to obtain the strain. On the one hand, diffraction measurements are sensitive to long-range order (within the coherence length of the beam) and so, when interstitials are generated inside the crystalline lattice, due to their positive formation volume, a lattice dilatation is observed. On the other hand, EXAFS is a well-suited method to extract the first NN distances averaged on the whole film and consequently it gives information about the lattice parameters in some crystallographic directions only at a local scale. This problem is in fact related with the already known difference between long-range order and short-range order: EXAFS is not a well-adapted method to probe long-range order and is not, compared to XRD, accurate enough for that aim up to now. This is clearly evidenced from the results we obtain when fitting bulk pure tungsten (Table I, Fig. 1): the second distance is shorter than its known lattice parameter of about 0.005 Å. Even if such a discrepancy is less than the actual EXAFS precision, it emphasizes the need for an improvement of the theory underlying the determination of the backscattering parameters (amplitude and phase shifts) to hope to obtain, using EXAFS, the level of accuracy achieved by XRD. Moreover, since we are measuring very small changes in the distances with orientation, one may ask if the angular averaging that cancels the contribution of the *s* channel to the EXAFS signal at the W L_3 edge is achieved as is implicitly assumed[54] in Eq. (10) because multilayers studied here are partially oriented (rocking curves FWHM: 9°). Nevertheless, we believe that we can safely use this equation, our samples being polycrystalline with small nearly cubic grains so that the angular averaging scheme is fulfilled. However, one cannot entirely reject a weak contribution of the *s* final state that may partially account for the difference we observe between EXAFS and XRD for distances at this edge. To end, considering a possible contribution of interstitials or clusters of defects with the EXAFS technique is still a challenge. Let us only remark that interstitial atoms being located at distances shorter than those of first near neighboring atoms, one can expect to observe a reduction of the now apparent NN distances. So, a significant contribution of interstitial-sites would be consistent with a reduction of the stress-free lattice parameter as well as with high DW factors' values.

The ion-induced stress relaxation effect observed for the Cu/W multilayers appears to be very similar to those quoted in recent papers where are reported tensile or compressive stress relaxation due to ion bombardment in thin metallic films such as W (Refs. 46,55) or Cr.[56] The stress relief is generally attributed to plastic flow effects, either via the nucleation and growth of dislocations,[57] or to a viscous flow in some glassy materials.[58] If little is known about the stress relaxation levels and on the dynamics of stress reduction, a kinetic dependence with the mass of the incident particle[38] has been clearly evidenced. Such a behavior tends to prove that relaxation effects are promoted by thermal spikes created inside collision cascades.[59] In good agreement with the model proposed by Jain *et al.*,[60] the present study suggests that stress relaxation under ion bombardment involves a clustering of self-interstitial atoms in interstitial dislocation loops.

IV. CONCLUSION

In this paper, we have presented an analysis of Cu/W multilayers elaborated by direct ion beam sputtering combining the EXAFS and XRD techniques. To summarize, both indicate that the as-deposited Cu/W multilayer is characterized by tungsten sublayers which structure is strained while the copper ones are found to be in a state close to pure fcc copper. An elasticity analysis of the EXAFS data yields an average in-plane compressive stress $\bar{\sigma} \sim -5.6$ (± 1.5) GPa in good agreement with the one deduced from XRD data [$\bar{\sigma} \sim -5.3$ (± 0.3) GPa]. For the largest part, this stress originates from an overall substrate-interaction stress and for a little part (less than one half of its value) from coherency stresses between W and Cu sublayers. Nevertheless, the free-stress lattice parameters obtained from EXAFS are systematically smaller than those measured from XRD (EXAFS: $a_0 \sim 3.157$ Å; XRD: $a_0 \sim 3.178$ Å). This discrepancy may be due to the intrinsic difference between short-range and long-range order probes, but also to not enough accurate backscattering parameters and a weak contribution of the *s* channel, a too high statistical noise in the EXAFS signals and/or to the impossibility, by principle, to include the contribution of point defects (interstitials or clusters) in the EXAFS

analysis. However, EXAFS yields additional informations compared to XRD about the structural disorder state of both components that makes these two techniques complementary to study stresses and strains in thin films. In particular, we have shown that the stress field present inside W sublayers is accompanied by a local positional disorder. It is maximum in the (110) W planes that are, from XRD results, parallel to the surface of the Cu/W superlattice. This increase of in-plane disorder can be ascribed to an epitaxial relationship between the bcc and fcc lattices. In the same way, the disorder is quite large into the Cu layers in the direction of growth owing to the presence of extended defects (twins, stacking faults) in this component of the multilayer.

We have also evidenced that ion irradiation turns out to be an efficient tool to modify the stress state of the multilayer. Indeed, it has been shown from both the EXAFS and XRD analysis that a large stress relief at half its starting value occurs inside W sublayers for a dose as low as 0.04 dpa. In turn, the ion irradiation does not modify the lattice parameter of the Cu layers. However, the EXAFS analysis evidences that ion irradiation induces atomic rearrangements in both components of the multilayer, this effect being particularly noticeable in-plane for the tungsten where we observe a significant reduction of the DW factors. To end, better insight about the structure of the superlattices studied here needs additional experiments using other techniques such as diffraction anomalous fine structure (DAFS) spectroscopy[61] which will be more suited than conventional EXAFS since it offers the advantage to combine XAFS-like information with resonant x-ray scattering and diffraction.

---

*Email address: Michel.Jaouen@univ-poitiers.fr

[1] For a review see, for example, I. K. Schuller, A. Fartasch, and M. Grimsditch, Mater. Res. Bull. **15**, 33 (1990); A. F. Jankowski, Nanostruct. Mater. **6**, 179 (1995).

[2] I. K. Schuller and M. Grimsditch, J. Vac. Sci. Technol. B **4**, 1444 (1986).

[3] I. K. Schuller and A. Rahman, Phys. Rev. Lett. **50**, 1377 (1983).

[4] M. L. Hubermann and M. Grimsditch, Phys. Rev. Lett. **50**, 1403 (1989).

[5] A. F. Jankowski and T. Tasalakos, J. Phys. F **15**, 1279 (1985).

[6] B. M. Clemens and G. L. Eesley, Phys. Rev. Lett. **61**, 2356 (1988).

[7] J. A. Jaszczak, S. R. Phillpot, and D. Wolf, J. Appl. Phys. **68**, 4573 (1990).

[8] J. A. Bain, L. J. Chyung, S. Brennan, and B. M. Clemens, Phys. Rev. B **44**, 1184 (1991).

[9] B. M. Clemens and J. A. Bain, Mater. Res. Bull. **17**, 46 (1992).

[10] J. A. Ruud, A. Witvrouw, and F. Spaepen, J. Appl. Phys. **74**, 2517 (1993).

[11] M. R. Scanton, R. C. Cammarata, D. Keavney, J. Freeland, J. C. Walker, and C. Hayzelden, Appl. Phys. Lett. **66**, 19 (1995).

[12] S. Labat, P. Gergaud, O. Thomas, B. Gilles, and A. Marty, J. Appl. Phys. **87**, 1172 (2000).

[13] Ph. Goudeau, K. F. Badawi, A. Naudon, and G. Gladyszewski, Appl. Phys. Lett. **62**, 1 (1993).

[14] E. Romanet, B. Bonnello, R. Gohier, J. C. Jeannet, and B. Perrin, J. Phys. IV **6**, 143 (1996).

[15] M. Maurer, M. Piecuch, M. F. Ravet, J. C. Ousset, J. P. Sanchez, C. Aaron, J. Decoster, D. Raoux, A. De Andres, M. De Santis, A. Fontaine, F. Beaudelet, J. L. Rouvière and B. Dieny, J. Magn. Magn. Mater. **93**, 15 (1991).

[16] H. Magnan, D. Chandesris, B. Villette, O. Heckmann, and J. Lecante, Phys. Rev. Lett. **67**, 859 (1991).

[17] S. Pizzini, F. Baudelet, D. Chandesris, A. Fontaine, H. Magnan, J. M. George, F. Petroff, A. Barthlemy, A. Fert, R. Loloee, and P. A. Schroeder, Phys. Rev. B **46**, 1253 (1992).

[18] S. Pizzini, F. Baudelet, A. Fontaine, M. Galtier, D. Renard, and C. Marlière, Phys. Rev. B **47**, 8754 (1993).

[19] S. K. Kim, Y. M. Koo, V. A. Chernov, and H. Padmore, Phys. Rev. B **53**, 11 114 (1996).

[20] P. Le Fèvre, H. Magnan, and D. Chandesris, Phys. Rev. B **54**, 2830 (1996).

[21] J. F. Ziegler, J. P. Biersack, and U. Littmark, in *The Stopping and Range of Ions in Matter* (Pergamon, New York, 1985).

[22] G. Gladyszewski, J. Pacaud, Ph. Goudeau, C. Jaouen, A. Naudon, and J. Grilhé, Vacuum **45**, 285 (1994).

[23] I. C. Noyan and J. B. Cohen in *Residual Stress: Measurement by Diffraction and Interpretation* (Springer, New York, 1987).

[24] V. Hauk, in *Structure and Residual Stress Analysis by Nondestrutive Methods* (Elsevier 1997).

[25] M. E. Kordesch and R. W. Hoffman, Phys. Rev. B **29**, 491 (1984).

[26] J. Mimault, J. J. Faix, T. Girardeau, M. Jaouen, and G. Tourillon, Meas. Sci. Technol. **5**, 482 (1994).

[27] B. K. Teo, in *EXAFS: Basic Principles and Data Analysis* (Springer, Berlin, 1986).

[28] A. Michalowicz, in *Logiciels pour la Chimie* (Society of French Chemistry, Paris, 1991).

[29] B. Lengeler and P. Eisenberger, Phys. Rev. B **21**, 4507 (1980).

[30] P. A. Lee and J. B. Pendry, Phys. Rev. B **11**, 2795 (1975).

[31] J. Stöhr in *X-Ray Absorption/ Principles, Applications, Techniques of EXAFS, SEXAFS and XANES*, edited by D.C. Koningsberger and R. Prins, Vol. 92 of *Chemical Analysis* (Wiley, New York, 1988).

[32] S. M. Heald and E. A. Stern, Phys. Rev. B **16**, 5549 (1977).

[33] C. Brouder, J. Phys.: Condens. Matter **2**, 701 (1990).

[34] R. B. Greegor and F. W. Lytle, Phys. Rev. B **20**, 4902 (1979).

[35] Nguyen Van Hung and J. J. Rehr, Phys. Rev. B **56**, 43 (1997).

[36] S. I. Zabinsky, J. J. Rehr, A. Ankudinov, R. C. Albers, and M. J. Eller, Phys. Rev. B **52**, 2995 (1995).

[37] G. G. Li, F. Bridges, and C. H. Booth, Phys. Rev. B **52**, 6332 (1995).

[38] K. F. Badawi, Ph. Goudeau, J. Pacaud, C. Jaouen, J. Delafond, A. Naudon, and G. Gladyszewski, Nucl. Instrum. Methods Phys. Res. B **80/81**, 404 (1993).

[39] B. K. Teo and P. A. Lee, J. Am. Chem. Soc. **101**, 2815 (1979).

[40] E. Bauer, H. Poppa, G. Todd, and F. Bonczek, J. Appl. Phys. **45**, 5164 (1974).

[41] L. A. Bruce and H. Jeager, Philos. Mag. A **38**, 223 (1978).

[42] J. Pacaud, Ph.D. thesis, Poitiers University, France, 1992.

[43] T. Girardeau, J. Mimault, M. Jaouen, P. Chartier, and G. Tourillon, Phys. Rev. B **46**, 7144 (1992).

[44] S. L. M. Schroeder, G. D. Moggrige, R. M. Lambert, and T. Rayment, J. Phys. IV **7**, 91 (1997).

[45] R. F. S. Hearmon, in *The Elastic Constants of Non-piezoelectric*

Crystals, *Landolt-Börnstein, Numerical Data and Relationships in Science and Technology* (Springer, Berlin, 1969).
[46] N. Durand, K. F. Badawi, Ph. Goudeau, and A. Naudon, J. Phys. III **4**, 45 (1994).
[47] F. M. d'Heurle and J. M. E. Harper, Thin Solid Films **171**, 185 (1989).
[48] F. Karetta and H. M. Urbassek, J. Appl. Phys. **71**, 5410 (1992).
[49] F. H. Streitz, R. C. Cammarata, and K. Sieradzki, Phys. Rev. B **49**, 10 707 (1994).
[50] B. J. Daniels, W. D. Nix, and B. J. Clemens, Appl. Phys. Lett. **66**, 2969 (1995).
[51] W. D. Nix, Metall. Trans. A **20**, 2217 (1989).
[52] C. Thompson, J. Mater. Res. **8**, 237 (1993).
[53] J. Pacaud, C. Jaouen, and G. Gladyszewski, J. Appl. Phys. **86**, 4847 (1999).
[54] J. Stöhr and R. Jaeger, Phys. Rev. B **27**, 5146 (1983).
[55] E. Snoeks, K. S. Boutros, and J. Barone, Appl. Phys. Lett. **71**, 267 (1997).
[56] A. Misra, S. Fayeulle, H. Kung, T. E. Mitchell, and M. Nastasi, Nucl. Instrum. Methods Phys. Res. B **148**, 42 (1999).
[57] B. Holländer, S. Mantl, R. Liedtke, S. Mesters, H. J. Herzog, H. Kibbel, and T. Hackbarth, Nucl. Instrum. Methods Phys. Res. B **148**, 200 (1999).
[58] E. Snoeks, T. Weber, A. Cacciato, and A. Polman, J. Appl. Phys. **78**, 4723 (1994).
[59] T. Diaz de la Rubia, R. S. Averbach, H. Hsieh, and R. J. Benedek, J. Mater. Res. **4**, 579 (1989).
[60] A. Jain, Scr. Metall. Mater. **32**, 589 (1994).
[61] H. Renevier, J. L. Hodeau, P. Wolfers, S. Andrieu, J. Weigelt, and R. Frahm, Phys. Rev. Lett. **78**, 2775 (1997).